

Spin correlation effects in top quark pair production at the LHC

Gregory Mahlon*

Penn State Mont Alto, 1 Campus Drive, Mont Alto, Pennsylvania 17237, USA

Stephen J. Parke[†]

Theoretical Physics Department, Fermi National Accelerator Laboratory, P.O. Box 500, Batavia, Illinois 60510, USA
(Received 2 February 2010; published 22 April 2010)

At a 14 TeV proton-proton collider, the Large Hadron Collider (LHC), we show that top quark pair production is dominated at low invariant mass by the fusion of two like-helicity gluons, producing top quark pairs in the left-left or right-right helicity configurations. Whereas, at higher invariant mass the production is dominated by the fusion of unlike-helicity gluons, producing top quark pairs in the up-down or down-up off-diagonal configurations, identical to top quark pair production via quark-antiquark annihilation. We study in detail the low invariant mass region, and show that the spin correlations can be easily observed in this region by looking at the distribution of the difference in the azimuthal angles, $\Delta\phi$, of the dileptons decay products of the top quarks in the laboratory frame. Because of the large cross section for top pair production at the LHC, even with a cut requiring that the invariant mass of the top quark pair be less than 400 GeV, the approximate yield would be 10^4 dilepton (e, μ) events per fb^{-1} before detector efficiencies are applied. Therefore, there is ample statistics to form the $\Delta\phi$ distribution of the dilepton events, even with the invariant mass restriction. We also discuss possibilities for observing these spin correlations in the lepton plus jets channel.

DOI: 10.1103/PhysRevD.81.074024

PACS numbers: 14.65.Ha

I. INTRODUCTION

Since the discovery of the top quark with a mass between 150 and 200 GeV¹ by the CDF and D0 experiments at Fermilab in 1995, numerous authors, see [2–10], have asked the question “Can the spin correlations in top quark pair production be observed?” This is a valid question since the top quark lifetime in the standard model is very short compared to the spin decorrelation time for such a heavy quark. In particular, $\Gamma_T \sim G_F m_t^3 \gg \Lambda_{\text{QCD}}^2/m_t$ where Γ_T is the total width of the top quark, m_t is mass of top quark, G_F is the Fermi constant and Λ_{QCD} is the QCD scale, thus the top quark decays before QCD interactions have the opportunity to appreciably affect its spin. The angular distribution of the top quark decay products in $t \rightarrow W^+ + b$ followed by $W^+ \rightarrow l^+ + \nu$ or $\bar{d} + u$ are correlated with the top spin axis as follows:

$$\frac{1}{\Gamma_T} \frac{d\Gamma}{d\cos\chi_i} = (1 + \alpha_i \cos\chi_i)/2$$

$$\alpha_i = \begin{cases} +1.0 & l^+ \text{ or } \bar{d}\text{-quark} \\ -0.31 & \bar{\nu} \text{ or } u\text{-quark} \\ -0.41 & b\text{-quark} \end{cases} \quad (1)$$

where χ_i is the angle between the i -th decay product and the top quark spin axis in the top quark rest frame. Clearly,

*gdm10@psu.edu

[†]parke@fnal.gov

¹The current Tevatron-averaged, best-fit value for the top quark mass is 173.1 ± 1.3 GeV, see Ref. [1].

the charged lepton or d -quark coming from the decay of the W -boson are the most correlated with the top quark spin axis. For the antitop, the signs of the α_i coefficients are flipped. Thus, if the spins of the top are correlated in top quark pair production and the decay products of the tops are correlated with the spins then the decay products of the two top quarks are correlated. Since there is no net polarization of the top quarks, at least to leading order, the correlation between the i -th decay product of the top and \bar{i} -th decay product of the antitop can be expressed by

$$\frac{1}{\sigma_T} \frac{d^2\sigma}{d\cos\chi_i d\cos\bar{\chi}_{\bar{i}}} = \frac{1}{4} (1 + C_{i\bar{i}} \alpha_i \bar{\alpha}_{\bar{i}} \cos\chi_i \cos\bar{\chi}_{\bar{i}}). \quad (2)$$

with

$$C_{i\bar{i}} \equiv \frac{\sigma_{\uparrow\uparrow} + \sigma_{\downarrow\downarrow} - \sigma_{\uparrow\downarrow} - \sigma_{\downarrow\uparrow}}{\sigma_{\uparrow\uparrow} + \sigma_{\downarrow\downarrow} + \sigma_{\uparrow\downarrow} + \sigma_{\downarrow\uparrow}}. \quad (3)$$

$\sigma_{\uparrow/\downarrow\uparrow/\downarrow}$ is the production cross section for top quark pairs where the top quark has spin up or down with respect to the top spin axis and the antitop has spin up or down with respect to the antitop spin axis. Clearly, the right choice for the spin axes of the top quark pair is important since a poor choice of spin axes can lead to a small value for the correlation parameter, $C_{i\bar{i}}$ and hence to small correlations between the decay products of the top and the antitop. For some processes, e.g. $q\bar{q} \rightarrow t\bar{t}$, there exist spin axis choices such that the correlation parameter, $C_{i\bar{i}}$, is maximal. However, even with these optimal choices, to observe the correlations one has to measure the angles χ_i and $\bar{\chi}_{\bar{i}}$ between the decay products and the spin axes in the rest frame of the top and antitop quarks, respectively. To do this

one has to reconstruct the top and the antitop rest frames; this is very challenging at a hadron collider. An obvious question is “Are there variables that carry the signature of the spin correlations which can be measured in the laboratory frame?” For $q\bar{q} \rightarrow t\bar{t}$ no such variables have been found that show a significant difference between full spin correlations and no spin correlations.

It has been known for some time that the spin correlations at the LHC are described very well by the helicity basis at low top-antitop invariant mass, whereas at higher invariant mass, counter to one’s naïve expectation, the spin correlations are degraded in the helicity basis. In this paper we explain this phenomenon by showing that at low invariant mass top quark pair production is dominated by like-helicity gluons, producing top quark pairs in the left-left or right-right helicity configuration, independent of the invariant mass. Whereas, at higher invariant mass top quark pair production is dominated by unlike-helicity gluons, producing top quark pairs in the up-down or down-up off-diagonal configuration, identical to that of top quark pair production via quark-antiquark annihilation. At ultrahigh invariant masses, the up-down and down-up off-diagonal configurations become the familiar left-right or right-left helicity configurations; however, at the LHC only a small fraction of the total number of produced top pair events are in this ultrahigh invariant mass region. The fact that the contributions from like and unlike-helicity gluons impart different spin correlations to the top quark pairs makes $gg \rightarrow t\bar{t}$, which dominates top quark pair production at the LHC, a much richer process for analysis than the dominant Tevatron mechanism $q\bar{q} \rightarrow t\bar{t}$.

We study the low invariant mass region in detail. In this region, the like-helicity gluons dominate the production. We show that the spin correlations can be easily observed in this region by looking at the distribution of the difference in the azimuthal angles, $\Delta\phi$, of the dilepton decay products of the top quarks. For top quark pairs with an invariant mass ≤ 400 GeV, the spin correlations give a 40% enhancement of this distribution at small angles ($\Delta\phi \approx 0$) and a 40% suppression of this distribution at large angles ($\Delta\phi \approx \pi$) compared to if there were no correlations between the production and decay of the top quarks. About 20% (~ 200 pb) of the total next-to-leading order top-antitop quark production cross section passes this invariant mass cut so even in the dilepton channel there are large numbers of events available to measure this distribution: about 10^4 events per fb^{-1} before detector efficiencies are applied.

The outline of this paper is as follows: in Sec. II we review what is known about the spin correlations for $q\bar{q} \rightarrow t\bar{t}$ before taking a closer look at the spin correlations for $gg \rightarrow t\bar{t}$ in Sec. III. Section IV addresses the question of how the top quark pair events at the LHC populate the scattering angle versus invariant mass plane. In Sec. V we add the decays of the top quarks. In Sec. VI we address the

issue of which angular distributions are sensitive to the presence or absence of angular correlations among the $t\bar{t}$ decay products. We show that at low invariant mass the difference in the azimuthal angle of the charged leptons carries the signature of spin correlations in the laboratory frame. We also discuss possibilities for observing these spin correlations in the lepton plus jets channel. We summarize our conclusions in Sec. VII. Last, we include an Appendix which outlines the highly efficient method used in this paper for calculating the spin amplitudes. It can be applied to any $2 \rightarrow 2$ process with arbitrary spins of the final state particles.

II. REVIEW OF $q\bar{q} \rightarrow t\bar{t}$

A. Spin amplitudes in an arbitrary basis

For a massive particle with momentum, t , and spin vector, s_t , the following relationships are satisfied

$$t^2 = m_t^2, \quad s_t^2 = -1, \quad \text{and} \quad t \cdot s_t = 0. \quad (4)$$

The spin vector s_t is most conveniently defined in the rest frame of the massive particle; in this frame it only can have spatial components. Thus, for top-antitop quark pair production via quark-antiquark annihilation or gluon-gluon fusion, we define the spin vector s_t in the rest frame of the top quark. Since CP is conserved at tree level for this process, we restrict the spin vector to be in the scattering plane. It is convenient to measure the direction of spin vector s_t with respect to the antitop quark or recoil direction. Thus we define the unit vector s_t such that its direction is at an angle ξ , measured clockwise with respect to the antitop quark direction (see Fig. 1).

For the antitop quark we proceed in a similar fashion in defining $s_{\bar{t}}$. Here, instead of using the same angle ξ to specify the direction of the spin vector with respect to the recoil direction, we use a different angle ξ' . This allows for the independent manipulation of the antitop and top quark

Top quark rest frame

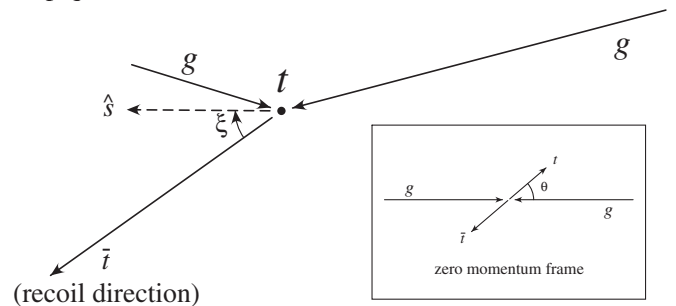


FIG. 1. Spin vector for top quark pair production. The direction of the top quark spin vector s_t is given by the angle ξ in this frame, measured in the clockwise direction from the recoil direction. The inset illustrates the situation in the ZMF, where the top and antitop are produced back-to-back and the scattering angle θ from the incoming beam direction.

spins at intermediate steps. However, in the end, we will set $\xi^l = \xi$: then, in the zero momentum frame (ZMF), the spin vectors of the top and antitop quark are back-to-back as expected from the symmetry arguments.

It is particularly convenient to use the following combinations of t and s_t as follows:

$$t_1 \equiv (t + m_t s_t)/2, \quad \text{and} \quad t_2 \equiv (t - m_t s_t)/2. \quad (5)$$

These satisfy

$$t_1^2 = t_2^2 = 0, \quad t = t_1 + t_2, \quad \text{and} \quad 2t_1 \cdot t_2 = m_t^2. \quad (6)$$

(\bar{t}_1 and \bar{t}_2 are defined similarly for the antitop quark.) Since t_1 and t_2 are lightlike vectors, the full power of the spinor helicity method can be used in evaluating the amplitudes as discussed in Ref. [11], resulting in many simplifications. For example, the Dirac spinor for a massive fermion with spin up can be written as, see [12]

$$U_\uparrow(t) = \frac{1 + \gamma_5}{2} U(t_1) + e^{i\Psi} \frac{1 - \gamma_5}{2} U(t_2). \quad (7)$$

This factorization into chiral components, with one depending only on t_1 and other only t_2 (apart from the phase factor $e^{i\Psi} \equiv \bar{U}(t_2) \frac{1+\gamma_5}{2} U(t_1)/m_t$), is particularly useful. For our purposes in this paper we need only two such spinors: a \bar{U}_\uparrow spinor for the top quark, and a V_\uparrow spinor for the antitop quark. These are given in spinor helicity notation by

$$\begin{aligned} \bar{U}_\uparrow(t) &= \langle t_1 + | + \frac{\langle t_1 + | t_2 - \rangle}{m_t} \langle t_2 - | = \frac{1}{m_t} \langle t_1 + | (t + m_t) \\ V_\uparrow(\bar{t}) &= |\bar{t}_1 - \rangle - |\bar{t}_2 + \rangle \frac{\langle \bar{t}_2 + | \bar{t}_1 - \rangle}{m_t} = (m_t - \bar{t}) |\bar{t}_1 - \rangle \frac{1}{m_t}. \end{aligned} \quad (8)$$

The full set of spinors for massive fermions may be found in Ref. [2]. In this paper we will show that once you have the amplitudes for $gg \rightarrow t_1 \bar{t}_1$ in terms of the spin angles ξ and ξ^l , you can obtain all of the other spin combinations for the top and antitop by simple algebraic manipulations.

B. Review of the spin structure of $q\bar{q} \rightarrow t\bar{t}$

The spinor structure of the matrix element for $q_R \bar{q}_L \rightarrow t\bar{t}$ can easily be shown to be of the form

$$\bar{U}(t) \{ |q+\rangle \langle \bar{q}+| + |\bar{q}-\rangle \langle q-| \} V(\bar{t}) \quad (9)$$

by using the Fierz identities on the current-current structure of the matrix element given by the standard Feynman rules. This can be used to recover the well-known tree-level matrix element squared for $q_R \bar{q}_L \rightarrow t\bar{t}$ (see Ref. [5]):

$$\begin{aligned} |\mathcal{A}(q_R \bar{q}_L \rightarrow t_1 \bar{t}_1 \text{ and } t_1 \bar{t}_1)|^2 &= |\mathcal{A}(q_L \bar{q}_R \rightarrow t_1 \bar{t}_1 \text{ and } t_1 \bar{t}_1)|^2 \\ &\sim (\gamma^{-1} \sin\theta \cos\xi - \cos\theta \sin\xi)^2 \\ |\mathcal{A}(q_R \bar{q}_L \rightarrow t_1 \bar{t}_1 \text{ or } t_1 \bar{t}_1)|^2 &= |\mathcal{A}(q_L \bar{q}_R \rightarrow t_1 \bar{t}_1 \text{ or } t_1 \bar{t}_1)|^2 \\ &\sim (\gamma^{-1} \sin\theta \sin\xi + \cos\theta \cos\xi \mp 1)^2. \end{aligned} \quad (10)$$

Here the same spin angle, ξ , has been used for both the top and antitop quarks. From this general result it is clear that there is a basis, defined by

$$\tan\xi = \gamma^{-1} \tan\theta, \quad (11)$$

which sets the $\uparrow\uparrow + \downarrow\downarrow$ component to identically zero for all β , leaving only the $\uparrow\downarrow + \downarrow\uparrow$ component. This basis was first identified by Parke and Shadmi in Ref. [5] and has been called the off-diagonal basis. It interpolates between the beamline basis ($\cos\xi = \cos\theta$) at threshold, and the helicity basis ($\cos\xi = \pm 1$) in the ultrarelativistic limit. In the off-diagonal basis, Eq. (10) becomes

$$\begin{aligned} |\mathcal{A}(q_R \bar{q}_L \rightarrow t_1 \bar{t}_1 \text{ and } t_1 \bar{t}_1)|^2 &= |\mathcal{A}(q_L \bar{q}_R \rightarrow t_1 \bar{t}_1 \text{ and } t_1 \bar{t}_1)|^2 \\ &= 0 \\ |\mathcal{A}(q_R \bar{q}_L \rightarrow t_1 \bar{t}_1 \text{ or } t_1 \bar{t}_1)|^2 &= |\mathcal{A}(q_L \bar{q}_R \rightarrow t_1 \bar{t}_1 \text{ or } t_1 \bar{t}_1)|^2 \\ &\sim (1 \mp \sqrt{1 - \beta^2 \sin^2\theta})^2, \end{aligned} \quad (12)$$

whereas the helicity basis is obtained by setting $\cos\xi = -1$; in this basis

$$\begin{aligned} |\mathcal{A}(q_R \bar{q}_L \rightarrow t_R \bar{t}_R \text{ and } t_L \bar{t}_L)|^2 &= |\mathcal{A}(q_L \bar{q}_R \rightarrow t_R \bar{t}_R \text{ and } t_L \bar{t}_L)|^2 \\ &\sim \gamma^{-2} \sin^2\theta \\ |\mathcal{A}(q_R \bar{q}_L \rightarrow t_R \bar{t}_L \text{ or } t_L \bar{t}_R)|^2 &= |\mathcal{A}(q_L \bar{q}_R \rightarrow t_L \bar{t}_R \text{ or } t_R \bar{t}_L)|^2 \\ &\sim (1 \pm \cos\theta)^2. \end{aligned} \quad (13)$$

Clearly, for $\gamma \gg 1$, the helicity basis and the off-diagonal basis become identical. As we will see in the next section, the spin correlations for unlike-helicity gluons producing top quark pairs are identical to those in quark-antiquark annihilation.

III. A CLOSER LOOK AT $gg \rightarrow t\bar{t}$

The tree-level matrix element for $gg \rightarrow t\bar{t}$ can be factorized into two terms: one depending on the color factors and t and u -channel propagators and the other depending on the spin of the gluons and top quarks, as follows

$$\mathcal{A}(g_1 g_2 \rightarrow t\bar{t}) = i g_s^2 \left[\frac{[T^{a_1} T^{a_2}]_{ii}}{(2t \cdot p_1)} + \frac{[T^{a_2} T^{a_1}]_{ii}}{(2t \cdot p_2)} \right] M(g_1 g_2 \rightarrow t\bar{t}). \quad (14)$$

The reduced matrix element $M(g_1 g_2 \rightarrow t\bar{t})$ is symmetric under the interchange of the two gluon momenta but depends on the helicity of the gluons and the spin of the top and antitop quarks.

The square of the color-propogator factor, summed over the gluon and top quark colors, is given by

$$\sum_{\text{color}} \left| \frac{[T^{a_1} T^{a_2}]_{ii}}{(2t \cdot p_1)} + \frac{[T^{a_2} T^{a_1}]_{ii}}{(2t \cdot p_2)} \right|^2 = \frac{4}{3} \frac{4(t \cdot p_1)^2 + 4(t \cdot p_2)^2 - (t \cdot p_1)(t \cdot p_2)}{(t \cdot p_1)^2 (t \cdot p_2)^2}. \quad (15)$$

When evaluated in the ZMF, this sum reduces to the form

$$\sum_{\text{color}} \left| \frac{[T^{a_1} T^{a_2}]_{ii}}{(2t \cdot p_1)} + \frac{[T^{a_2} T^{a_1}]_{ii}}{(2t \cdot p_2)} \right|^2 = \frac{\mathcal{Y}(\beta, c_\theta)}{\gamma^4 m_t^4}, \quad (16)$$

with

$$\mathcal{Y}(\beta, c_\theta) = \frac{4}{3} \frac{7 + 9\beta^2 c_\theta^2}{(1 - \beta^2 c_\theta^2)^2}. \quad (17)$$

In these expressions β is the ZMF speed of the top quarks and c_θ is the cosine of the ZMF scattering angle θ .

The reduced matrix element for on-mass-shell top quarks, $M(g_R g_L \rightarrow t\bar{t})$, is simply given by

$$M(g_R g_L \rightarrow t\bar{t}) = \frac{2\langle p_2 + |t|p_1 + \rangle}{2p_1 \cdot p_2} \times \bar{U}(t)\{\langle p_1 + | \langle p_2 + | + |p_2 - \rangle \langle p_1 - | \} V(\bar{t}) \quad (18)$$

for unlike-helicity gluons and by

$$M(g_R g_R \rightarrow t\bar{t}) = 2m_t \frac{\langle p_1 - |p_2 + \rangle}{\langle p_1 + |p_2 - \rangle} \bar{U}(t)\gamma_L V(\bar{t}) \quad (19)$$

$$\text{where } \gamma_{L,R} \equiv \frac{1}{2}(1 \mp \gamma_5)$$

for like-helicity gluons. Note the similarity in the spinor structure for $g_R g_L \rightarrow t\bar{t}$ and $q_R \bar{q}_L \rightarrow t\bar{t}$. Also, the spinor structure for $g_R g_R \rightarrow t\bar{t}$ is particularly simple, $\bar{U}(t)\gamma_L V(\bar{t})$; it contains no s -channel pole. In a later section of this paper, we use these two expressions to give a simple analytic expression for $gg \rightarrow t\bar{t}$ including the decay of the two top quarks. However, in the next section we will evaluate these expressions using the spinors for polarized top quarks given in Eq. (8).

A. Unlike-helicity gluons

For unlike-helicity gluons the reduced matrix element $M(g_R g_L \rightarrow t_1 \bar{t}_1)$ is given by

$$M(g_R g_L \rightarrow t_1 \bar{t}_1) = \frac{2\langle p_2 + |t|p_1 + \rangle}{m_t(2p_1 \cdot p_2)} \times \{ \langle t_1 + |t_2|p_1 + \rangle \langle p_2 + | \bar{t}_1 - \rangle - \langle t_1 + |p_2 - \rangle \langle p_1 - | \bar{t}_1 - \rangle \}, \quad (20)$$

which, when evaluated in the ZMF using the spin vectors described in the previous section, becomes

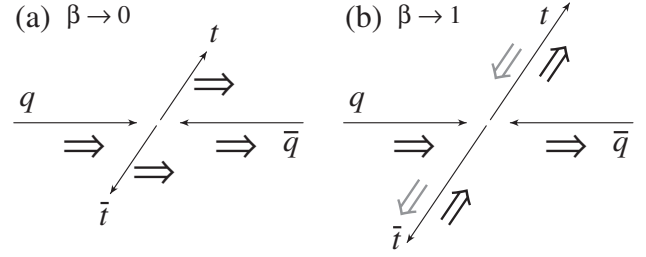


FIG. 2. The spin configurations for the process $q_R \bar{q}_L \rightarrow t\bar{t}$ are best described by the off-diagonal basis which interpolates between the beam line basis at low β to helicity at very high β as given by Eq. (12). (a) is the limit $\beta \rightarrow 0$ where the top quark spins are aligned in the same direction as the incoming quark spins whereas (b) is the limit $\beta \rightarrow 1$ where the helicity state $t_R \bar{t}_L$ dominates for scattering angles less than 90 degrees. The relative probability of $t_R \bar{t}_L$ to $t_L \bar{t}_R$ is given by $(1 + \cos\theta)^2 : (1 - \cos\theta)^2$.

$$M(g_R g_L \rightarrow t_1 \bar{t}_1) \sim \beta \sin\theta \{ (1 - \cos\theta) \sin(\xi/2) \cos(\xi'/2) - (1 + \cos\theta) \cos(\xi/2) \sin(\xi'/2) + \gamma^{-1} \sin\theta [\cos(\xi/2) \cos(\xi'/2) - \sin(\xi/2) \sin(\xi'/2)] \}. \quad (21)$$

Here the coefficients in front of the products of the ξ -dependent trigonometric functions are the appropriate helicity amplitudes whereas the products of the ξ -dependent trigonometric functions themselves are products of Wigner d -functions (see Appendix A). The relative signs between the various components of these expressions are important and care must be taken to make sure they are correct.

Using a different spin angle for the t and \bar{t} allows for manipulation of the spin of the top independent of the antitop and vice versa. Thus, all of the spin amplitudes for $g_R g_L \rightarrow t\bar{t}$ can be simply obtained from $g_R g_L \rightarrow t_1 \bar{t}_1$ as follows:

$$|M_{\uparrow\uparrow}(\xi, \xi')| = |M_{\uparrow\uparrow}(\xi \pm \pi, \xi')| = \left| \left(\frac{d}{d\xi/2} \right) M_{\uparrow\uparrow}(\xi, \xi') \right| \quad (22)$$

$$|M_{\uparrow\uparrow}(\xi, \xi')| = |M_{\uparrow\uparrow}(\xi, \xi' \pm \pi)| = \left| \left(\frac{d}{d\xi'/2} \right) M_{\uparrow\uparrow}(\xi, \xi') \right| \quad (23)$$

$$|M_{\uparrow\downarrow}(\xi, \xi')| = |M_{\uparrow\downarrow}(\xi \pm \pi, \xi' \pm \pi)| = \left| \left(\frac{d}{d\xi/2} \right) \left(\frac{d}{d\xi'/2} \right) M_{\uparrow\uparrow}(\xi, \xi') \right|. \quad (24)$$

Flipping the spin of a particle is accomplished by one of two equivalent methods:

- (i) Addition or subtraction of π from the spin angle ξ .
- (ii) Differentiation of the amplitude with respect to $\xi/2$.

A detailed discussion with examples of how to use these techniques for arbitrary spins is given in Appendix A.

At this stage we can make the spin axes of the top quark pair back-to-back in the ZMF by setting $\xi' = \xi$. Thus, for

unlike-helicity gluons we obtain

$$|\mathcal{A}(g_R g_L \rightarrow t_1 \bar{t}_1 \text{ and } t_1 \bar{t}_1)|^2 = \mathcal{Y}(\beta, \theta) \beta^2 \sin^2 \theta \times (\gamma^{-1} \sin \theta \cos \xi - \cos \theta \sin \xi)^2, \quad (25)$$

$$|\mathcal{A}(g_R g_L \rightarrow t_1 \bar{t}_1 \text{ or } t_1 \bar{t}_1)|^2 = \mathcal{Y}(\beta, \theta) \beta^2 \sin^2 \theta \times (\gamma^{-1} \sin \theta \sin \xi + \cos \theta \cos \xi \mp 1)^2, \quad (26)$$

and

$$|\mathcal{A}(g_L g_R \rightarrow t_1 \bar{t}_1 \text{ and } t_1 \bar{t}_1)|^2 = |\mathcal{A}(g_R g_L \rightarrow t_1 \bar{t}_1 \text{ and } t_1 \bar{t}_1)|^2, \quad (27)$$

$$|\mathcal{A}(g_L g_R \rightarrow t_1 \bar{t}_1 \text{ or } t_1 \bar{t}_1)|^2 = |\mathcal{A}(g_R g_L \rightarrow t_1 \bar{t}_1 \text{ or } t_1 \bar{t}_1)|^2, \quad (28)$$

with

$$\sum_{\text{all}} |\mathcal{A}(g_R g_L \rightarrow t\bar{t})|^2 = \sum_{\text{all}} |\mathcal{A}(g_L g_R \rightarrow t\bar{t})|^2 = 2\mathcal{Y}(\beta, \theta) \beta^2 \sin^2 \theta (2 - \beta^2 \sin^2 \theta). \quad (29)$$

As in $q\bar{q} \rightarrow t\bar{t}$, a great simplification occurs for the off-diagonal basis [5], $\tan \xi = \gamma^{-1} \tan \theta$, where

$$|\mathcal{A}(g_L g_R \rightarrow t_1 \bar{t}_1 \text{ and } t_1 \bar{t}_1)|^2 = |\mathcal{A}(g_R g_L \rightarrow t_1 \bar{t}_1 \text{ and } t_1 \bar{t}_1)|^2 = 0. \quad (30)$$

The off-diagonal basis is the basis that interpolates from the beamline basis at threshold to the helicity bases at ultrarelativistic energies for the $q\bar{q} \rightarrow t\bar{t}$ process. Thus, for unlike-helicity gluons we have a very similar situation to that of $q\bar{q} \rightarrow t\bar{t}$: the only nonzero amplitudes are given by

$$|\mathcal{A}(g_R g_L \rightarrow t_1 \bar{t}_1 \text{ or } t_1 \bar{t}_1)|^2 = |\mathcal{A}(g_L g_R \rightarrow t_1 \bar{t}_1 \text{ or } t_1 \bar{t}_1)|^2 = \mathcal{Y}(\beta, \theta) \beta^2 \sin^2 \theta \times (1 \mp \sqrt{1 - \beta^2 \sin^2 \theta})^2, \quad (31)$$

as illustrated in Fig. 3.

B. Like-helicity gluons

For like-helicity gluons the reduced matrix element $M(g_R g_R \rightarrow t_1 \bar{t}_1)$ is simply given by the following combination of spinor products

$$M(g_R g_R \rightarrow t_1 \bar{t}_1) = 2m_t \frac{\langle p_1 - | p_2 + \rangle}{\langle p_1 + | p_2 - \rangle} \langle t_1 + | \bar{t}_1 - \rangle, \quad (32)$$

which when evaluated in the ZMF using the spin vectors described in the previous section is just

$$M(g_R g_R \rightarrow t_1 \bar{t}_1) \sim \gamma^{-1} \{ (1 - \beta) \cos(\xi/2) \cos(\xi'/2) + (1 + \beta) \sin(\xi/2) \sin(\xi'/2) \}. \quad (33)$$

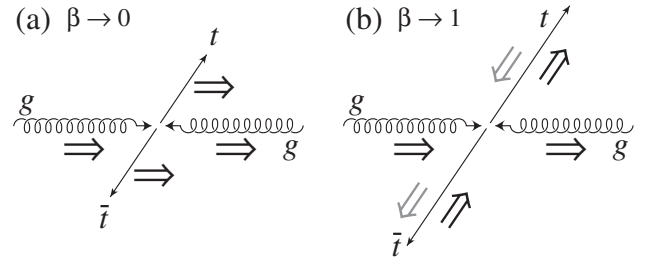


FIG. 3. The spin configurations for the process $g_R g_L \rightarrow t\bar{t}$ are best described by the off-diagonal basis, which interpolates between the beamline basis at low β and the helicity basis at very high β [see Eq. (31)]. As far as the spins of the top quarks are concerned, this process, $g_R g_L \rightarrow t\bar{t}$, is identical to top quark production via quark-antiquark collisions, $q_R \bar{q}_L \rightarrow t\bar{t}$, see Fig. 2. (a) illustrates the limit $\beta \rightarrow 0$ where the top quark spins are aligned in the same direction as the incoming gluon spins whereas (b) illustrates the limit $\beta \rightarrow 1$ where the helicity state $t_R \bar{t}_L$ dominates for scattering angles less than 90 degrees. The relative probability of $t_R \bar{t}_L$ to $t_L \bar{t}_R$ is given by $(1 + \cos \theta)^2 : (1 - \cos \theta)^2$.

Treating these expressions in a manner similar to the unlike-helicity case discussed in the previous section we obtain

$$|\mathcal{A}(g_R g_R \rightarrow t_1 \bar{t}_1 \text{ or } t_1 \bar{t}_1)|^2 = \mathcal{Y}(\beta, \theta) \gamma^{-2} (1 \mp \beta \cos \xi)^2, \quad (34)$$

$$|\mathcal{A}(g_R g_R \rightarrow t_1 \bar{t}_1 \text{ and } t_1 \bar{t}_1)|^2 = \mathcal{Y}(\beta, \theta) \gamma^{-2} \beta^2 \sin^2 \xi. \quad (35)$$

Similarly, it is easy to show that for left-handed like-helicity gluons

$$|\mathcal{A}(g_L g_L \rightarrow t_1 \bar{t}_1 \text{ or } t_1 \bar{t}_1)|^2 = |\mathcal{A}(g_R g_R \rightarrow t_1 \bar{t}_1 \text{ or } t_1 \bar{t}_1)|^2, \quad (36)$$

$$|\mathcal{A}(g_L g_L \rightarrow t_1 \bar{t}_1 \text{ and } t_1 \bar{t}_1)|^2 = |\mathcal{A}(g_R g_R \rightarrow t_1 \bar{t}_1 \text{ and } t_1 \bar{t}_1)|^2. \quad (37)$$

Summing over all of the final spins gives

$$\sum_{\text{all}} |\mathcal{A}(g_R g_R \rightarrow t\bar{t})|^2 = \sum_{\text{all}} |\mathcal{A}(g_L g_L \rightarrow t\bar{t})|^2 = 2\mathcal{Y}(\beta, \theta) (1 - \beta^4), \quad (38)$$

independent of the spin axis used for the top quarks.

Clearly, a great simplification occurs for like-helicity gluons if one uses the helicity basis ($\xi = 0$ or π) for the top quarks. In the helicity basis

$$|\mathcal{A}(g_L g_L \rightarrow t_R \bar{t}_L \text{ and } t_L \bar{t}_R)|^2 = |\mathcal{A}(g_R g_R \rightarrow t_R \bar{t}_L \text{ and } t_L \bar{t}_R)|^2 = 0 \quad (39)$$

for all values of β . Conventional wisdom states that helicity provides a simple description for most processes only at ultrarelativistic energies. However, as illustrated in Fig. 4, $t\bar{t}$ production from like-helicity gluons is an exception to this expectation: in this case, the helicity basis provides a simple description for all β , with the only nonzero amplitudes given by

$$|\mathcal{A}(g_R g_R \rightarrow t_R \bar{t}_R \text{ or } t_L \bar{t}_L)|^2 = |\mathcal{A}(g_L g_L \rightarrow t_L \bar{t}_L \text{ or } t_R \bar{t}_R)|^2 = \mathcal{Y}(\beta, \theta) \gamma^{-2} (1 \pm \beta)^2. \quad (40)$$

Both the like and unlike gluon helicity amplitudes agree with those found in the appendix of Ref. [13].

C. Combining like- and unlike-helicity gluons

At the LHC we must combine the like-helicity and unlike-helicity gluon cases since there is no way to polarize the incoming gluons. By looking at Eqs. (26) and (35), it is clear that there is no basis which makes the top quark spins purely $\uparrow\uparrow + \downarrow\downarrow$ OR $\uparrow\downarrow + \downarrow\uparrow$ at the LHC because the constant term appears in $\uparrow\uparrow + \downarrow\downarrow$ for like-helicity gluons and in $\uparrow\downarrow + \downarrow\uparrow$ for unlike-helicity gluons.

However, there are regions of the $(\cos\theta, \beta)$ plane for which the like-helicity gluon amplitude or the unlike-helicity amplitude dominates. Along the curve given by

$$\beta\gamma \sin\theta = 1 \quad \text{or, equivalently,} \quad \beta^2 = 1/(2 - \cos^2\theta) \quad (41)$$

the like-helicity and the unlike-helicity contribute equally to top quark pair production. On this curve

$$\begin{aligned} \sum_{\text{all}} |\mathcal{A}(g_R g_R \rightarrow t\bar{t})|^2 &= \sum_{\text{all}} |\mathcal{A}(g_L g_L \rightarrow t\bar{t})|^2 \\ &= \sum_{\text{all}} |\mathcal{A}(g_R g_L \rightarrow t\bar{t})|^2 \\ &= \sum_{\text{all}} |\mathcal{A}(g_L g_R \rightarrow t\bar{t})|^2. \end{aligned}$$

$$f(\theta, \beta) \equiv \frac{\sum_{\uparrow\uparrow+\downarrow\downarrow} |\mathcal{A}(gg \rightarrow t\bar{t})|^2}{\sum_{\text{all}} |\mathcal{A}(gg \rightarrow t\bar{t})|^2} = \frac{\gamma^{-2}(1 + \beta^2 \cos^2\xi) + \beta^2 \sin^2\theta (\gamma^{-1} \sin\theta \cos\xi - \cos\theta \sin\xi)^2}{(1 - \beta^4) + \beta^2 \sin^2\theta (2 - \beta^2 \sin^2\theta)}.$$

It is a straightforward analytic exercise² to find the extrema of this function with respect to the angle ξ . The maxima, $f_{\text{same}}(\theta, \beta)$, gives the maximum fraction of $\uparrow\uparrow + \downarrow\downarrow$ whereas the minima, $f_{\text{oppo}}(\theta, \beta)$, gives the minimum fraction of $\uparrow\uparrow + \downarrow\downarrow$ or, equivalently, the maximum fraction of $\uparrow\downarrow + \downarrow\uparrow$. These fractions are given by

$$f_{\{\text{same, oppo}\}}(\theta, \beta) \equiv \frac{\gamma^{-2} + \frac{1}{2}\beta^2(\sin^2\theta \cos^2\theta + \gamma^{-2} \sin^4\theta + \gamma^{-2}) \{1 \pm \sqrt{1 - \frac{(2\gamma^{-1} \cos\theta \sin\theta)^2}{(\sin^2\theta \cos^2\theta + \gamma^{-2} \sin^4\theta + \gamma^{-2})}}\}}{(1 - \beta^4) + \beta^2 \sin^2\theta (2 - \beta^2 \sin^2\theta)}. \quad (42)$$

Both extrema occur when ξ satisfies

$$\tan 2\xi_{\{\text{same, oppo}\}} = \frac{2\gamma^{-1} \sin^3\theta \cos\theta}{\sin^2\theta \cos^2\theta - \gamma^{-2} \sin^4\theta - \gamma^{-2}}; \quad (43)$$

they are related as follows: $\xi_{\text{oppo}} = \xi_{\text{same}} + \pi/2$. The contours of $f_{\text{same}}(\theta, \beta)$ in the $(\cos\theta, \beta^2)$ plane are given by the solid lines in Fig. 5(a) whereas for $f_{\text{oppo}}(\theta, \beta)$ see Fig. 5(b).

At any given point in the $(\cos\theta, \beta^2)$ plane, the basis which exhibits the strongest correlations is the one whose spin fraction has the largest difference from $\frac{1}{2}$. If

²The numerical solution was studied in Ref. [14].

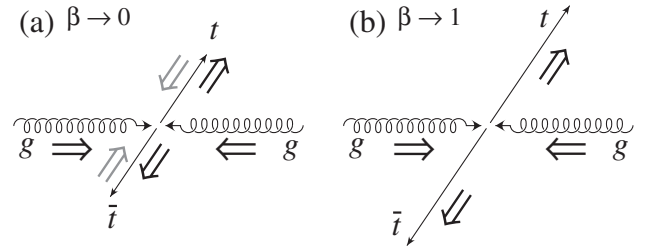


FIG. 4. The spin configurations for the process $g_R g_R \rightarrow t\bar{t}$ are best described by the helicity basis for all β [see Eq. (40)]. (a) illustrates the limit $\beta \rightarrow 0$ where the relative probability of $t_R \bar{t}_R$ to $t_L \bar{t}_L$ is $(1 + \beta)^2 : (1 - \beta)^2$ whereas (b) illustrates the limit $\beta \rightarrow 1$ where $t_R \bar{t}_R$ completely dominates. For $g_L g_L \rightarrow t\bar{t}$, flip the spins on both the gluons and the top quarks.

In the region $\beta\gamma \sin\theta < 1$ the like-helicity gluon amplitudes dominate the cross section, whereas in the region $\beta\gamma \sin\theta > 1$ the unlike-helicity gluon amplitudes dominate the cross section. Thus, it is clear that one should use the helicity basis when $\beta\gamma \sin\theta \ll 1$ and the off-diagonal basis when $\beta\gamma \sin\theta \gg 1$. In the next section we will optimize the basis choice to maximize the spin correlations in the intermediate region, $\beta\gamma \sin\theta \sim 1$.

D. Optimizing the choice of spin basis

For unpolarized gluons, the fraction of top quark pair events at a given point in the $(\cos\theta, \beta)$ plane that have $\uparrow\uparrow$ or $\downarrow\downarrow$ spins is

$|f_{\text{oppo}}(\theta, \beta) - 1/2|$ is larger than $|f_{\text{same}}(\theta, \beta) - 1/2|$ then one should use ξ_{oppo} ; otherwise, ξ_{same} should be used. The condition that must be satisfied for both $f_{\text{same}}(\theta, \beta)$ and $f_{\text{oppo}}(\theta, \beta)$ to have equal difference (but opposite sign) from $1/2$ occurs when

$$f_{\text{same}}(\theta, \beta) + f_{\text{oppo}}(\theta, \beta) = 1, \quad \text{or} \quad \beta\gamma \sin\theta = 1. \quad (44)$$

Not surprisingly this is the same curve that also separates the dominance of the contribution of like-helicity from unlike-helicity gluons. Thus, when $\beta\gamma \sin\theta < 1$ the like-helicity gluons dominate and ξ_{same} should be used to maximize the $\uparrow\uparrow + \downarrow\downarrow$ fraction, whereas if $\beta\gamma \sin\theta > 1$ the unlike-helicity gluons dominate and we should use ξ_{oppo}

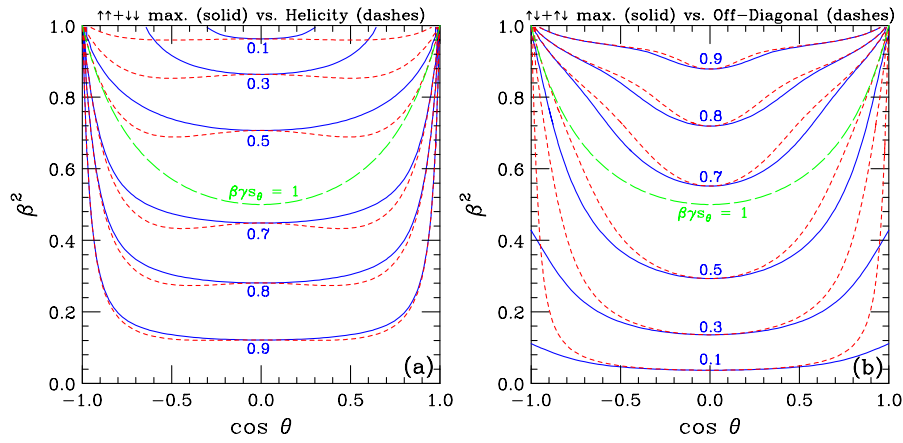


FIG. 5 (color online). Panels (a) and (b) show, in the $(\cos\theta, \beta^2)$ plane, the maximum fractions of $\uparrow\uparrow + \downarrow\downarrow$, $f_{\text{same}}(\theta, \beta)$, and $\uparrow\downarrow + \downarrow\uparrow$, $f_{\text{oppo}}(\theta, \beta)$, respectively, (solid contours). In both panels the long-dashed line is $\beta\gamma\sin\theta = 1$ or equivalently $\beta^2 = 1/(2 - \cos^2\theta)$ below which the like-helicity gluons dominate and above the unlike-helicity gluons dominate. In (a) the short-dashed lines are the fractions of $LL + RR$ top quark pairs in the helicity basis which below $\beta\gamma\sin\theta = 1$ are close to the maximum fractions for $\uparrow\uparrow + \downarrow\downarrow$, $f_{\text{same}}(\theta, \beta)$. Whereas in (b) the short-dashed lines are the fractions of $\uparrow\downarrow + \downarrow\uparrow$ in the Off-Diagonal basis which above $\beta\gamma\sin\theta = 1$ are close to the maximum fractions of $\uparrow\downarrow + \downarrow\uparrow$, $f_{\text{oppo}}(\theta, \beta)$.

to maximize the $\uparrow\downarrow + \downarrow\uparrow$ fraction; this is equivalent to minimizing the $\uparrow\uparrow + \downarrow\downarrow$ fraction. The long-dashed line in both parts of Fig. 5 is the curve $\beta\gamma\sin\theta = 1$; this is the demarcation curve between maximizing $\uparrow\uparrow + \downarrow\downarrow$ and maximizing $\uparrow\downarrow + \downarrow\uparrow$.

It is worthwhile asking the following two questions:

- (i) In the region dominated by like-helicity gluons ($\beta\gamma\sin\theta < 1$), how much does the maximum fraction of $\uparrow\uparrow + \downarrow\downarrow$ differ from what the helicity basis would give in the same region?
- (ii) In the region dominated by unlike-helicity gluons ($\beta\gamma\sin\theta > 1$), how much does the maximum fraction of $\uparrow\downarrow + \downarrow\uparrow$ differ from what the off-diagonal basis would give in the same region?

These two questions are also addressed by Fig. 5. In (a) we have also plotted (short dashes) the fraction of top quark pairs which are $LL + RR$ in the helicity basis and in (b) the fraction that are $\uparrow\downarrow + \downarrow\uparrow$ in the off-diagonal basis. Clearly, these figures indicate that the helicity basis does almost as well as the basis which maximizes $\uparrow\uparrow + \downarrow\downarrow$ for $\beta\gamma\sin\theta < 1$ and that the off-diagonal basis does almost as well as the basis which maximizes $\uparrow\downarrow + \downarrow\uparrow$ for $\beta\gamma\sin\theta > 1$.

Now that we understand the production dynamics for top quark pair production from gluon-gluon fusion we can turn to the question of what regions in the $(\cos\theta, \beta^2)$ plane do the top quark pair events occur at the LHC.

IV. PHENOMENOLOGY OF TOP QUARK PAIR PRODUCTION AT THE LHC

In Fig. 6 we plot the differential cross section

$$\frac{1}{\sigma_{\text{tot}}} \frac{d^2\sigma}{d(\cos\theta)d\beta^2}(gg \rightarrow t\bar{t})$$

in the $(\cos\theta, \beta^2)$ plane where σ_{tot} is the total cross section.

This figure gives us the relative distribution of top quark pair events in this plane. A breakdown of the fraction of events for like- and unlike-helicity gluons broken into the appropriate regions in $\beta\gamma s_\theta$ are given in Table I.

Figure 7 shows the differential cross section with respect to $|C_{\text{same}}|$, where

$$C_{\text{same}} \equiv 2f_{\uparrow\uparrow+\downarrow\downarrow} - 1 \quad \text{and} \quad C_{\text{oppo}} \equiv 2f_{\uparrow\downarrow+\downarrow\uparrow} - 1 \quad (45)$$

are the quantities which control the size of the correlations for any given spin basis (note that $C_{\text{oppo}} = -C_{\text{same}}$). In this

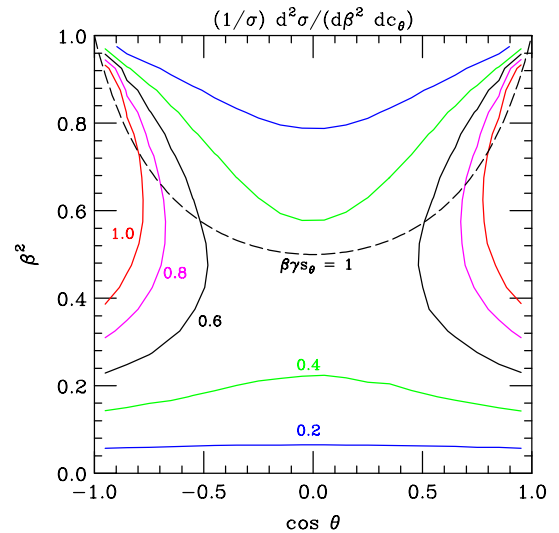


FIG. 6 (color online). The differential cross section $(1/\sigma_{\text{tot}})d^2\sigma/d(\cos\theta)d\beta^2$ for top quark pair production at the LHC assuming total beam energy of 14 TeV. The long-dashed line is $\beta\gamma\sin\theta = 1$ (or $\beta^2 = 1/(2 - \cos^2\theta)$) is the demarcation line for the differential cross section to be dominated by like-helicity gluons (below) and unlike-helicity gluons (above).

TABLE I. Fraction of $t\bar{t}$ events categorized by the helicities of the initial state gluons and location in the $(\cos\theta, \beta^2)$ plane at the LHC with $\sqrt{s} = 14$ TeV.

	$\beta\gamma s_\theta < 1$	$\beta\gamma s_\theta > 1$	all
gg Like	55%	10%	65%
gg Unlike	20%	15%	35%
Total	75%	25%	100%

figure we have split up the contributions into two pieces: one for $\beta\gamma \sin\theta < 1$ and the other for $\beta\gamma \sin\theta \geq 1$. For $\beta\gamma \sin\theta < 1$, we show the contribution in the basis which maximizes the $\uparrow\uparrow + \downarrow\downarrow$ component as well as the helicity basis; whereas for $\beta\gamma \sin\theta \geq 1$, we show the contribution in the basis which maximizes $\uparrow\downarrow + \downarrow\uparrow$ as well as the off-diagonal basis. This figure clearly shows that there are only small differences between using the best basis and the helicity basis for $\beta\gamma \sin\theta < 1$ and the best basis and the off-diagonal basis for $\beta\gamma \sin\theta > 1$.

At the LHC, the total top quark pair production cross section is ~ 1 nb (at next-to-leading order) giving approximately $10^6 t\bar{t}$ per fb^{-1} ; therefore, significant cuts can be made on the data before the statistical uncertainties become comparable to the systematic uncertainties. Thus, we will concentrate on the low β region for the rest of this paper since in this region like-helicity gluons dominate the production cross section and the boost of the top quarks does not mask the spin correlations.

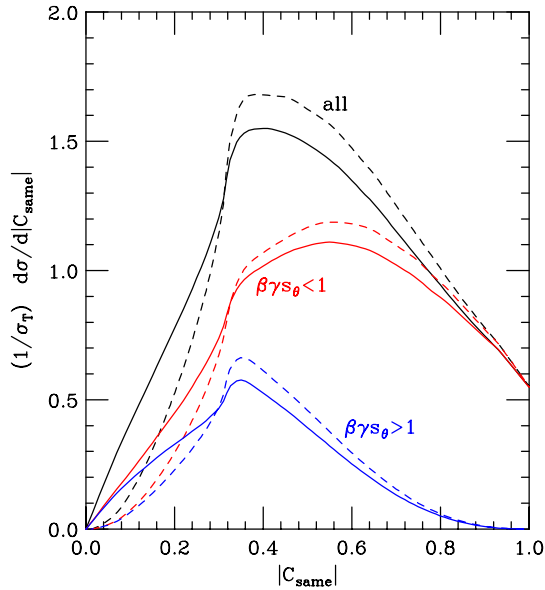


FIG. 7 (color online). The differential distributions of $|C_{\text{same}}|$, $(1/\sigma_T)d\sigma/d|C_{\text{same}}|$. The dashed curves are for the optimal basis, Eq. (43), whereas the solid curves employ the helicity basis when $\beta\gamma s_\theta < 1$ and the off-diagonal basis when $\beta\gamma s_\theta > 1$. The mean values of $|C_{\text{same}}|$ for the different bases and regions are collected in Table II.

V. ADDING TOP QUARK DECAYS

From Eqs. (18) and (19), it is easy to add the decays of the on mass shell top quarks, $t \rightarrow b + \bar{e} + \nu$ and $\bar{t} \rightarrow \bar{b} + \mu + \bar{\nu}$, via the following replacements:

$$\begin{aligned} \bar{U}(t) &\rightarrow \frac{g_w^2}{(2\bar{e} \cdot \nu - m_w^2 + im_w\Gamma_w)(im_t\Gamma_t)} \\ &\times \langle b - |\nu\rangle \langle \bar{e} + |t + m_t\rangle \\ V(\bar{t}) &\rightarrow (-\bar{t} + m_t)|\mu\rangle \langle \bar{\nu} + |\bar{b}\rangle \\ &\times \frac{g_w^2}{(2\mu \cdot \bar{\nu} - m_w^2 + im_w\Gamma_w)(im_t\Gamma_t)}. \end{aligned} \quad (46)$$

The Fierz identity has been employed in the derivation of these replacements. Thus, the total matrix element squared for top quark production and decay via gluon fusion, summed over the colors of the incoming gluons and outgoing b -quarks, is given by

$$\begin{aligned} |\mathcal{A}|_{RL}^2 + |\mathcal{A}|_{LR}^2 &= \mathcal{K} \left\{ \frac{2(p_1 \cdot t)(p_2 \cdot t) - m_t^2(p_1 \cdot p_2)}{(p_1 \cdot p_2)^2} \right\} \\ &\times \{ 2(t \cdot \bar{e})(\bar{t} \cdot \mu)[(p_1 \cdot t)^2 + (p_2 \cdot t)^2] \\ &- m_t^2[(p_1 \cdot p_2)((t \cdot \bar{e})(t \cdot \mu) \\ &+ (\bar{t} \cdot \bar{e})(\bar{t} \cdot \mu) - m_t^2(\bar{e} \cdot \mu)) \\ &- 2((p_1 \cdot t)(p_1 \cdot \mu)(p_2 \cdot \bar{e}) \\ &+ (p_2 \cdot t)(p_1 \cdot \bar{e})(p_2 \cdot \mu) \\ &- (p_1 \cdot t)(p_2 \cdot t)(\bar{e} \cdot \mu))] \} \end{aligned} \quad (47)$$

for unlike-helicity gluons, whereas for like-helicity gluons we have

$$\begin{aligned} |\mathcal{A}|_{RR}^2 + |\mathcal{A}|_{LL}^2 &= \mathcal{K} m_t^4 \{ (t \cdot \bar{e})(t \cdot \mu) + (\bar{t} \cdot \bar{e})(\bar{t} \cdot \mu) \\ &- m_t^2(\bar{e} \cdot \mu) \}. \end{aligned} \quad (48)$$

The overall factor \mathcal{K} is given by

$$\begin{aligned} \mathcal{K} &= \frac{2^6 g_s^4}{3} \frac{g_w^8}{(m_t\Gamma_t)^4} \\ &\times \left\{ \frac{4(p_1 \cdot t)^2 + 4(p_2 \cdot t)^2 - (p_1 \cdot t)(p_2 \cdot t)}{(p_1 \cdot t)^2(p_2 \cdot t)^2} \right\} \\ &\times \frac{b \cdot \nu}{(2\bar{e} \cdot \nu - m_w^2)^2 + (m_w\Gamma_w)^2} \\ &\times \frac{\bar{b} \cdot \bar{\nu}}{(2\mu \cdot \bar{\nu} - m_w^2)^2 + (m_w\Gamma_w)^2}. \end{aligned} \quad (49)$$

Appendix B contains the corresponding expressions describing $q\bar{q} \rightarrow t\bar{t}$.

Notice the simplicity of the matrix element squared for like-helicity gluons to top quark pairs. Given this simplicity and the fact that the like-helicity gluon contribution dominated at smaller values of the invariant mass of the $t\bar{t}$

TABLE II. Mean values of $|C_{\text{same}}|$ using either the optimal or appropriate choice of off-diagonal or helicity basis for events with different values of $\beta\gamma s_\theta$ at the LHC with $\sqrt{s} = 14$ TeV.

Basis	$\beta\gamma s_\theta < 1$	$\beta\gamma s_\theta > 1$	all
Optimal basis	0.55	0.59	0.43
Helicity or off-diagonal	0.53	0.57	0.39

system, it is worth exploring whether or not the full matrix element enhances the spin correlations in this channel.

The ratio of the correlated to uncorrelated³ matrix element squared, \mathcal{S} , for like-helicity gluons is given by

$$\begin{aligned}
\mathcal{S} &\equiv \frac{(|\mathcal{A}|_{RR}^2 + |\mathcal{A}|_{LL}^2)_{\text{corr}}}{(|\mathcal{A}|_{RR}^2 + |\mathcal{A}|_{LL}^2)_{\text{uncorr}}} \\
&= \frac{m_t^2 \{ (t \cdot \bar{e})(t \cdot \mu) + (\bar{t} \cdot \bar{e})(\bar{t} \cdot \mu) - m_t^2 (\bar{e} \cdot \mu) \}}{(t \cdot \bar{e})(\bar{t} \cdot \mu)(t \cdot \bar{t})} \\
&= \left(\frac{1 - \beta^2}{1 + \beta^2} \right) \left(\frac{(1 + \beta^2) + (1 - \beta^2)c_{\bar{e}\mu} - 2\beta^2 c_{t\bar{e}} c_{\bar{t}\mu}}{(1 - \beta c_{t\bar{e}})(1 - \beta c_{\bar{t}\mu})} \right),
\end{aligned} \tag{50}$$

where the last line is given in the ZMF in terms of speed of the tops, β , and the cosine of the angles between t and \bar{e} ($c_{t\bar{e}}$), \bar{t} and μ ($c_{\bar{t}\mu}$) and \bar{e} and μ ($c_{\bar{e}\mu}$). The range of \mathcal{S} is between (2, 0). At threshold, $\beta \rightarrow 0$, the maximum of \mathcal{S} occurs when the charged leptons are parallel, $c_{\bar{e}\mu} = +1$, whereas the minimum occurs when the charged leptons are back-to-back, $c_{\bar{e}\mu} = -1$, independent of their correlation with the top-antitop axis.

For nonzero β , the maximum (minimum) still occurs when the charged leptons are parallel (back-to-back), but they are now correlated with the top-antitop axis. The fact that the charged leptons are more likely to have their momenta being parallel rather than back-to-back is what is expected for top quark pairs that have spins which are antialigned, i.e. LL or RR . However, here the enhancement is even stronger than what one would naively expect because the interference between LL and RR strengthens the correlation between the momenta of the two charged leptons. This argument suggests looking at the ΔR , $\Delta \eta$ and $\Delta \phi$ distributions of the two charged leptons with a cut on the invariant mass of the top-antitop system.

³We call the decay of a top or antitop quark into a W -boson and b -quark uncorrelated if this decay is spherical in the top quark rest frame and thus independent of the top quark spin. The W -boson is then assumed to decay in the usual (fully-correlated) manner. The uncorrelated matrix elements squared are then given by $(|\mathcal{A}|_{RR}^2 + |\mathcal{A}|_{LL}^2)_{\text{uncorr}} = \mathcal{K}(t \cdot \bar{e})(\bar{t} \cdot \mu)\{m_t^2(t \cdot \bar{t})\}$ and $(|\mathcal{A}|_{RL}^2 + |\mathcal{A}|_{LR}^2)_{\text{uncorr}} = \mathcal{K}(t \cdot \bar{e})(\bar{t} \cdot \mu)\{[2(p_1 \cdot t)(p_2 \cdot t) - m_t^2(p_1 \cdot p_2)][(p_1 \cdot t)^2 + (p_2 \cdot t)^2 + m_t^2(p_1 \cdot p_2)]/(p_1 \cdot p_2)^2\}$.

VI. CORRELATION-SENSITIVE ANGULAR DISTRIBUTIONS

A. $\Delta \phi$ Distribution in dilepton events

In Fig. 8 we have plotted the $\Delta \phi$ distribution in the dilepton channel for $t\bar{t}$ production incorporating a cut which restricts the true invariant mass of the $t\bar{t}$ pair to less than 400 GeV. This plot shows results for both the fully-correlated and the uncorrelated matrix elements including both $gg \rightarrow t\bar{t}$ and $q\bar{q} \rightarrow t\bar{t}$ channels. A clear distinction between the correlated and uncorrelated decays⁴ is seen in this figure: the difference between the two $\Delta \phi$ distributions is about 40% at both $\Delta \phi = 0$ (enhancement) and $\Delta \phi = \pi$ (suppression). With this cut, 10% of the total cross section for $t\bar{t}$ production survives at leading order.

Unfortunately, the presence of the two neutrinos in the final state of dilepton events complicates the selection of events. The available kinematic constraints leave an up to 8-fold ambiguity⁵ in the reconstruction of the neutrino momenta from the available observed momenta and energies. Given the ease of measuring the azimuthal angles of charged leptons, it is worthwhile to investigate an alternative to the true $t\bar{t}$ invariant mass cut.

The simplest option one could imagine is to simply take the (naïve) unweighted average $\langle m_{t\bar{t}} \rangle$ of all of the real solutions returned by the neutrino reconstruction algorithm. In Fig. 9 we present the results of implementing just that option: the cut used to generate this figure requires that $\langle m_{t\bar{t}} \rangle$ be less than 400 GeV. With this cut approximately 5% of the total cross section for $t\bar{t}$ production survives at leading order. This is smaller than the fraction passing a 400 GeV cut on the true value of $m_{t\bar{t}}$ since only those events where all the spurious solutions are sufficiently small will survive. On the other hand, the sample passing this cut will contain a few events where the true value of $m_{t\bar{t}}$ is above 400 GeV, but, because the spurious solutions produced smaller values, the average was below 400 GeV. Turning to the $\Delta \phi$ distribution and comparing to the cut on the true value of $m_{t\bar{t}}$, one sees a rather large effect on the shape of the distributions. However, this effect (an enhancement near $\Delta \phi = 0$ and a depletion near $\Delta \phi = \pi$) occurs for *both* the correlated and uncorrelated data sets. Thus the difference between the two distributions remains at roughly the 40% level. No effort has been to optimize this invariant mass cut. Perhaps there are other variables that will do better than unweighted average $\langle m_{t\bar{t}} \rangle$,

⁴The corresponding $\Delta \eta$ distribution shows almost no difference between correlated and uncorrelated matrix elements. Thus all the difference in the ΔR distributions comes from the $\Delta \phi$ distributions.

⁵The presence of a pair of quadratic constraints in the kinematic equations leads to up to 4 solutions for any given pairing of the b jets with the two charged leptons. Since there are two possible pairings, as many as 8 different solutions could result. However, not all of these solutions need be real, and so there are often fewer than the maximum possible number of solutions.

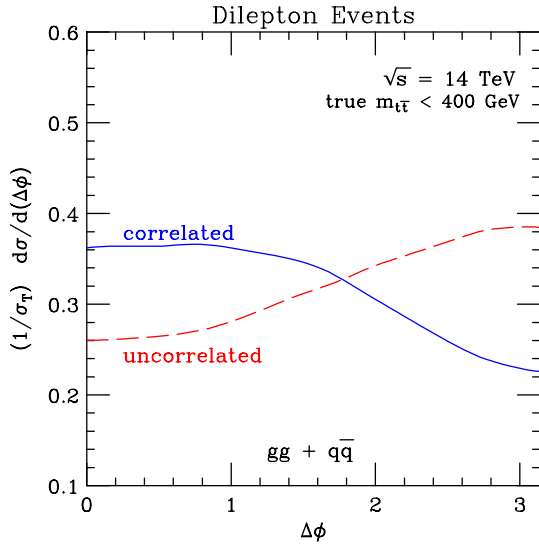


FIG. 8 (color online). The differential distribution of $\Delta\phi$, $(1/\sigma_T)d\sigma/d(\Delta\phi)$. The solid curve is for the fully-correlated case whereas the dashed curve assumes that the top quarks decay spherically in their respective rest frames. A cut restricting the invariant mass of the $t\bar{t}$ pairs to a maximum of 400 GeV has been applied to these distributions.

or perhaps 400 GeV is not the optimal cut value. Nevertheless, what we have here is a proof-in-principle that these correlations can be measured in an experiment.

B. ZMF $\cos\theta$ distribution for lepton-plus-jets events

Turning to the lepton-plus-jets channel, we have found that the cosine of the opening angle between the charged

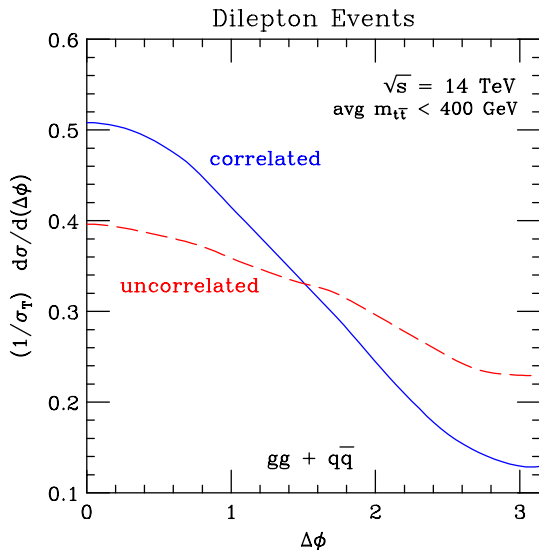


FIG. 9 (color online). The differential distribution of $\Delta\phi$, $(1/\sigma_T)d\sigma/d(\Delta\phi)$. The solid curve is for the fully-correlated case whereas the dashed curve assumes that the top quarks decay spherically in their respective rest frames. A cut restricting the average reconstructed invariant mass of the $t\bar{t}$ pairs to a maximum of 400 GeV has been applied to these distributions.

lepton and the d -quark jet as viewed in the zero momentum frame (ZMF) is sensitive to the presence or absence of correlations between production and decay [see also the discussion near Eq. (50)]. For this type of event the kinematic constraints provide more equations than unknowns. Thus, the ZMF may be reconstructed without ambiguity more than 98% of the time by discarding those solutions which do not pass some rudimentary quality-control cuts: the neutrino energy ought to be positive in a correctly reconstructed event; furthermore, the neutrino and top quark mass-shell constraints ought to be satisfied to sufficient accuracy.⁶ Discarding the $\sim 2\%$ of events that have more than one viable reconstruction of the ZMF is an acceptable option.

For the purposes of generating this distribution, we define the d -quark jet to be the jet which is spatially the closest to the b -tagged jet in the W rest frame, as was used in Ref. [2]. This is equivalent to using the lowest energy jet in the top quark rest frame as advocated in Ref. [15]. Figure 10 displays the results for this distribution using only those events that pass the cut $m_{t\bar{t}} < 400$ GeV. For fully-correlated top decays this distribution is nearly flat, whereas for spherical decays there is a strong peaking near $\cos\theta = -1$. That is, because of the correlations between production and decay, the lepton and the d -jet tend to be significantly less back-to-back in the ZMF than if no such correlations were present. Approximately 9% of the total cross section for $t\bar{t}$ production survives this cut at leading order, even at reduced center-of-mass energy.

C. Varying the energy of the LHC

So far we have used 14 TeV for the energy of the LHC. However, it is now clear that the LHC will not reach this energy for a number of years so we have investigated what happens for a reduced center-of-mass energy in this section. The results we describe below are summarized in Fig. 11.

The primary result of a lower center-of-mass energy is a big reduction in the $t\bar{t}$ production cross section because of the reduced gluon luminosity. Panel (a) in Fig. 11 tracks the leading order cross section from 7 to 14 TeV center-of-mass energy. We see that a factor of 2 reduction in \sqrt{s} produces a reduction of about a factor of 5 in the $t\bar{t}$ production cross section. Panel (b) illustrates the fact that the fraction of dilepton and lepton plus jet events surviving the $m_{t\bar{t}}$ or $\langle m_{t\bar{t}} \rangle$ cut we advocate does not change very much as \sqrt{s} is varied between 7 and 14 TeV. Finally, in panel (c) of each figure we compare the quantity $\mathcal{A}_{1/2}$, which is defined as half of the area between the correlated and

⁶Because of jet energy measurement uncertainties, it is not expected that a correctly reconstructed top quark or neutrino will be precisely on-mass-shell. The exact definition of “sufficient precision” is therefore a detector-dependent issue to be determined by the experimental collaborations.

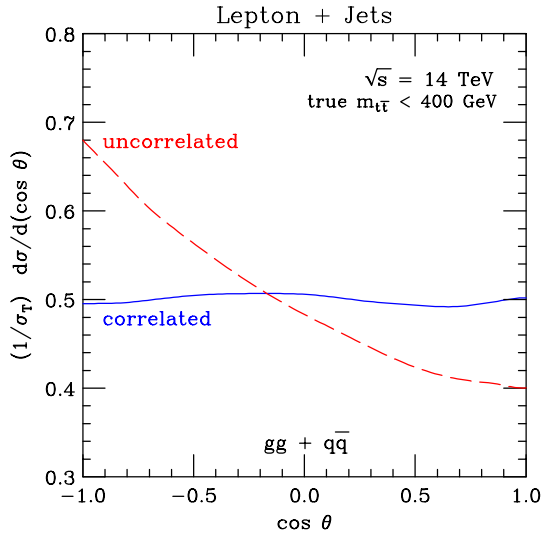


FIG. 10 (color online). The differential distribution of $\cos\theta$, $(1/\sigma_T)d\sigma/d(\cos\theta)$, where θ is the ZMF angle between the charged lepton and the d -quark jet (defined to be the jet which is spatially the closest to the b -tagged jet in the W rest frame; this is also the jet with the lowest energy in the top quark rest frame). The solid curve is for the fully-correlated case whereas the dashed curve assumes that the top quarks decay spherically in their respective rest frames. A cut restricting the invariant mass of the $t\bar{t}$ pairs to a maximum of 400 GeV has been applied to these distributions.

uncorrelated predictions for the unit-normalized angular distributions. This quantity ranges from 0 in the case where the distribution is completely independent of whether or not correlations are present up to 1 in the case where the two distributions (correlated decays or spherical decays) do not overlap at all. In both channels, there is relatively little dependence on \sqrt{s} for this measure of the difference between the correlated and spherical cases. Thus, the biggest issue related to the observation of these spin correlations at the LHC running at reduced energy comes from the greatly diminished cross section: the correlations themselves remain at roughly the same level. Fortunately, even a reduction of the number of $t\bar{t}$ pairs estimated in the introduction by a factor of 5 leaves ample statistics to hope for at least a preliminary observation of these spin correlation effects, even at reduced center-of-mass energy.

D. NLO Effects

Higher-order QCD effects enhance the total cross section especially near threshold. However, previous studies on $e^+e^- \rightarrow t\bar{t}$ demonstrate that such corrections to the spin correlations are small, see Ref. [16]. One can understand this physically since the emission of soft gluons from a top quark cannot flip the spin of the top quark. We have done a preliminary study of the NLO effects using both MCFM, [17] and MC@NLO, [18], incorporating a cut which restricts the invariant mass of the $t\bar{t}$ pair to be less than 400 GeV. Both these Monte Carlos show that the tree-level

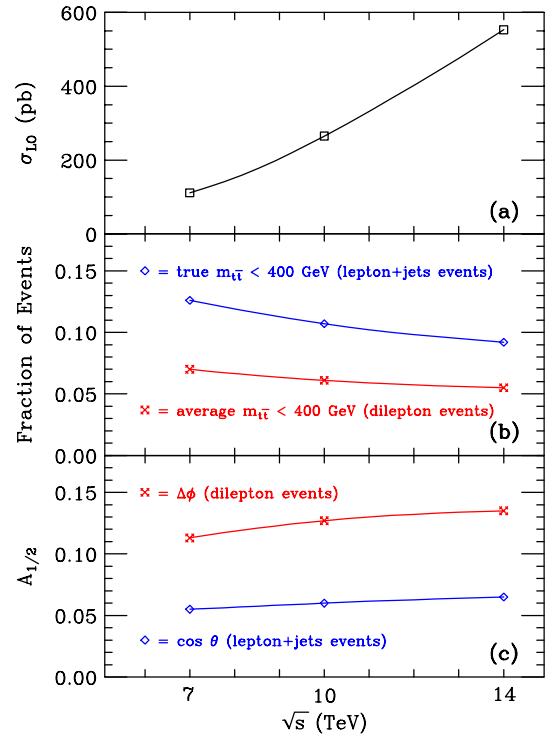


FIG. 11 (color online). Effects of varying the machine center-of-mass energy \sqrt{s} . (a) Total leading order cross section for $pp \rightarrow t\bar{t}$. These values should be multiplied by the branching fraction to dileptons (4.6%) or lepton-plus-jets (29%), as appropriate. We include only the e and μ channels. (b) Fraction of dilepton and lepton plus events with $m_{t\bar{t}} < 400$ GeV. For dilepton events (crosses) we employ the unweighted average of the up to 8 solutions for the $t\bar{t}$ invariant mass. For lepton + jets events (diamonds) the true value of $m_{t\bar{t}}$ may be reconstructed and used in event selection. (c) Half of the area between the appropriate unit-normalized angular distributions for the fully correlated and spherical cases. For lepton + jets events (crosses), we use the distribution in $\cos\theta$, where θ is the angle between the charged lepton and the d -jet candidate in the zero momentum frame of the event. For dilepton events (diamonds), we use the azimuthal opening angle $\Delta\phi$ between the two charged leptons.

effects discussed earlier in this paper are also present at NLO.⁷ We did not check the Monte Carlo of Ref. [19] which is the most complete NLO Monte Carlo to date, as there is no publicly available version at this time. A detailed study at NLO where the invariant mass of the $t\bar{t}$ pair is reconstructed from the decay products is beyond the scope of this work.

VII. SUMMARY AND CONCLUSIONS

In this paper we have shown how to observe spin correlations in top quark pair production at the LHC. To our surprise, the observation of these correlations is easier at

⁷In Fig. 1 of Ref. [18] one can see the size of the correlations without the invariant mass cut.

the LHC than at the Tevatron. The reason for this is that at the LHC the dominant production mechanism for top quark pairs is gluon-gluon fusion, which at low \hat{s} is dominated by the fusion of like-helicity pair gluons. The fusion of like-helicity gluons produces top quark pairs in a LL or RR helicity configuration. When such top quarks decay, they produce charged leptons which possess very strong azimuthal correlations. These correlations can be easily seen in the laboratory frame once a cut on the invariant mass of the top quark pair is made. There is no need to reconstruct the top quark rest frame as is required to see the correlations of top quark pairs at the Tevatron. The analysis has been extended to the lepton-plus-jets channel by “identifying” which jet is the d -quark jet from the W -boson decay on a statistical basis. Apart from the reduction of the total cross section, the size of these spin correlations is approximately independent of the energy of the LHC in the 7 to 14 TeV range. Thus, we expect that these effects could be observed in early running of the LHC.

ACKNOWLEDGMENTS

S. P. would like to thank Jiro Kodaira for many enlightened discussions over the course of many years. John Campbell, Keith Ellis, Stefano Frixione and Brian Webber are acknowledged for fruitful discussions about the NLO comparison. S. P. also thanks the CERN Theory group for hospitality during the “Top Quark Physics Institute” during May of 2009. G. M. would like to thank the Fermilab Theory group for its kind hospitality during multiple summer visits to concentrate on this work. Fermilab is operated by the Fermi Research Alliance under contract no. DE-AC02-07CH11359 with the U.S. Department of Energy.

APPENDIX A: UNIVERSAL PROPERTIES OF THE SPIN AMPLITUDES

In this Appendix we demonstrate the properties of the spin amplitudes and their relationship to the Wigner d -functions and the helicity amplitudes. Of particular importance is the fact that spin amplitudes at either end of the spin chain contain all the information necessary to obtain all the other spin amplitudes by simple algebraic manipulations. This fact was used extensively earlier in this paper.

1. Wigner d -functions and connection to the spin amplitudes

The amplitude for production of a single massive particle with spin j and spin-projection m in the generalized spin basis described in Sec. II A and illustrated in Fig. 1 may be written as a linear superposition of the matrix elements of the rotation operator [20]:

$$\mathcal{A}_{j,m}(\xi) \equiv \langle \vec{x} | jm \rangle_{\xi} = \sum_{m'} d_{m,m'}^j(-\xi) H_{m'}. \quad (\text{A1})$$

The $d_{m,m'}^j$ appearing in Eq. (A1) are the Wigner d -functions, chosen to conform to the conventions of Rose [21]. In particular, we write $-\xi$ since our angle ξ is measured in the clockwise direction whereas the angle β in Ref. [21] is counterclockwise. Since

$$d_{m,m'}^j(0) = \delta_{m,m'}, \quad (\text{A2})$$

we see that

$$H_m = \mathcal{A}_{j,m}(0). \quad (\text{A3})$$

That is, the coefficients H_m are the conventional helicity amplitudes for the process with a particular choice of relative phases.

Similarly, the production of a pair of massive particles (spins j_1 and j_2 , spin projections m_1 and m_2 along independent spin axes oriented at the clockwise angles ξ and ξ' with respect to the recoil direction in the scattering plane) may be decomposed as

$$\mathcal{A}_{j_1,m_1,j_2,m_2}(\xi, \xi') = \sum_m \sum_{m'} d_{m_1,m}^{j_1}(-\xi) d_{m_2,m'}^{j_2}(-\xi') H_{m,m'}. \quad (\text{A4})$$

The extension to more than two particles in the final state or to spin axes which point out of the production plane, involving the introduction of the Wigner D -functions in place of the (simpler) d -functions, is straightforward, but beyond the scope of this appendix.

2. $\xi \rightarrow \xi \pm \pi$ rule

Intuitively, we expect that the probability for producing spin-projection $+m$ along some axis ought to be equal to that for producing spin-projection $-m$ along minus that axis:

$$|\mathcal{A}_{j,m}(\xi \pm \pi)| = |\mathcal{A}_{j,-m}(\xi)|. \quad (\text{A5})$$

That is, flipping the z component of the spin and rotation by $\pm \pi$ give the same results up to a phase. This feature of the spin amplitudes is a consequence of the properties of the Wigner d -functions appearing in Eqs. (A1) and (A4).

3. Differential relations among the spin amplitudes

Consider a state with total spin j and projection $j_z = m$ in the general spin basis illustrated in Fig. 1. Applying the rotation operator converts this to a state where the spin axis is at $\xi + \Delta\xi$ instead [20]:

$$\mathcal{A}_{j,m}(\xi + \Delta\xi) = e^{i\Delta\xi J_y} \mathcal{A}_{j,m}(\xi). \quad (\text{A6})$$

In the limit $\Delta\xi \rightarrow 0$ Eq. (A6) may be rewritten as

$$\frac{\partial}{\partial \xi} \mathcal{A}_{j,m}(\xi) = \frac{1}{2} (J_+ - J_-) \mathcal{A}_{j,m}(\xi). \quad (\text{A7})$$

In this expression, we have replaced J_y by the appropriate linear combination of raising and lowering operators. Thus

$$\begin{aligned} \frac{\partial}{\partial \xi} \mathcal{A}_{j,m}(\xi) &= \frac{1}{2} \sqrt{j(j+1) - m(m+1)} \mathcal{A}_{j,m+1}(\xi) \\ &\quad - \frac{1}{2} \sqrt{j(j+1) - m(m-1)} \mathcal{A}_{j,m-1}(\xi) \end{aligned} \quad (\text{A8})$$

4. Starting at top or bottom of spin chain

It is useful to record the explicit results of applying Eq. (A8) to the ends of the spin chain:

$$\mathcal{A}_{j,\pm(j-1)}(\xi) = \mp \sqrt{\frac{2}{j}} \frac{\partial}{\partial \xi} \mathcal{A}_{j,\pm j}(\xi). \quad (\text{A9})$$

A second differentiation allows us to conclude that

$$\mathcal{A}_{j,\pm(j-2)}(\xi) = \frac{1}{\sqrt{j(2j-1)}} \left[j + 2 \frac{\partial^2}{\partial \xi^2} \right] \mathcal{A}_{j,\pm j}(\xi). \quad (\text{A10})$$

This process could be repeated as many times as required. However, when used in conjunction with the $\xi \rightarrow \xi \pm \pi$ rule of Eq. (A5), (A9), and (A10) allow the calculation of all of the amplitudes in the spin chain for spins up to and including $\frac{5}{2}$, starting from either end of the chain ($m = \pm j$). The relative simplicity of the operations involved in these relations makes for a substantial computational savings over the calculation of the complete set of amplitudes by direct means. Of course, once you have all the spin amplitudes then the helicity amplitudes can be easily obtained, including relative phases, by setting $\xi = 0$.

Thus, the spin amplitudes at the top and bottom of the spin chain contain all the information about a given process and all other spin amplitudes and helicity amplitudes can be derived from them. This special property of these spin amplitudes is simply reflected in the Wigner d -functions, $d_{j,m}^l$ for $m = \{-j, \dots, j\}$, which form a set of $(2j+1)$ linearly independent functions [22].

5. Examples

An explicit illustration of the relationships contained in Eqs. (A9) and (A10) is provided by the $gg \rightarrow t\bar{t}$ process considered in this paper. After setting $\xi' = \xi$ (back-to-back spin axes in the ZMF), we can organize the amplitudes according to the total spin in the final state. In doing this we need to keep in mind that for this choice of spin axes, *unlike* spin $t\bar{t}$ pairs have spins that point in the same spatial direction. Thus

$$|\mathcal{A}_{1,1}(\xi)| = |\mathcal{A}(gg \rightarrow t_1\bar{t}_1)| \quad (\text{A11})$$

and

$$|\mathcal{A}_{1,-1}(\xi)| = |\mathcal{A}(gg \rightarrow t_1\bar{t}_{-1})|. \quad (\text{A12})$$

The ξ -dependent linear combination of the $\uparrow\uparrow$ and $\downarrow\downarrow$ amplitudes must be $\mathcal{A}_{1,0}$; the orthogonal (ξ -independent) combination is $\mathcal{A}_{0,0}$:

$$|\mathcal{A}_{1,0}(\xi)| = \frac{1}{\sqrt{2}} |\mathcal{A}(gg \rightarrow t_1\bar{t}_1) + \mathcal{A}(gg \rightarrow t_1\bar{t}_{-1})|, \quad (\text{A13})$$

$$|\mathcal{A}_{0,0}(\xi)| = \frac{1}{\sqrt{2}} |\mathcal{A}(gg \rightarrow t_1\bar{t}_1) - \mathcal{A}(gg \rightarrow t_1\bar{t}_{-1})|. \quad (\text{A14})$$

For like-helicity gluons Eqs. (31) and (32) lead to

$$\begin{aligned} |\mathcal{A}_{1,1}(\xi)| &\sim \gamma^{-1} |\beta s_\xi| \\ |\mathcal{A}_{1,0}(\xi)| &\sim \sqrt{2} \gamma^{-1} |\beta c_\xi| \quad \text{and} \quad |\mathcal{A}_{0,0}(\xi)| \sim \sqrt{2} \gamma^{-1}. \\ |\mathcal{A}_{1,-1}(\xi)| &\sim \gamma^{-1} |\beta s_\xi| \end{aligned} \quad (\text{A15})$$

The three $j = 1$ amplitudes in (A15) satisfy

$$|\mathcal{A}_{1,0}(\xi)| = \left| \sqrt{2} \frac{\partial}{\partial \xi} \mathcal{A}_{1,1}(\xi) \right| \quad (\text{A16})$$

and

$$|\mathcal{A}_{1,-1}(\xi)| = \left| \left[1 + 2 \frac{\partial^2}{\partial \xi^2} \right] \mathcal{A}_{1,1}(\xi) \right| \quad (\text{A17})$$

as implied by Eqs. (A9) and (A10).

A different realization of these relationships is provided by the unlike-helicity gluons for which Eqs. (22) and (23) lead to

$$\begin{aligned} |\mathcal{A}_{1,1}(\xi)| &\sim \beta s_\theta (1 + c_\theta c_\xi + \gamma^{-1} s_\theta s_\xi) \\ |\mathcal{A}_{1,0}(\xi)| &\sim \sqrt{2} \beta s_\theta |c_\theta s_\xi - \gamma^{-1} s_\theta c_\xi| \quad \text{and} \quad |\mathcal{A}_{0,0}(\xi)| = 0. \\ |\mathcal{A}_{1,-1}(\xi)| &\sim \beta s_\theta (1 - c_\theta c_\xi - \gamma^{-1} s_\theta s_\xi) \end{aligned} \quad (\text{A18})$$

This is identical (up to overall factors) to what happens for the processes $q\bar{q} \rightarrow t\bar{t}$ and similar to what happens for $e^+e^- \rightarrow t\bar{t}$ [5]. The spin amplitudes for $e^+e^- \rightarrow Zh$ [23,24] also satisfy Eqs. (A16) and (A17).

Finally, we have verified that the processes $e^+e^- \rightarrow W^+W^-$ and ZZ provide examples of the $j = 2$ versions of Eqs. (A9) and (A10). Indeed, the derivative relations between the spin amplitudes for these processes noted in Ref. [23] are a direct consequence of Eq. (A9).

APPENDIX B: THE PROCESS $q\bar{q} \rightarrow t\bar{t}$

For completeness we give here the matrix element squared for $q\bar{q} \rightarrow t\bar{t}$ with the subsequent decay of the top quarks. Starting from Eq. (9) and using the substitutions given in Eq. (46), it is easy to add the decays of the on-mass-shell top quarks ($t \rightarrow b + \bar{e} + \nu$ and $\bar{t} \rightarrow \bar{b} + \mu + \bar{\nu}$). Thus, the total matrix element squared for top quark production and decay via quark-antiquark annihilation, summed over the colors of the incoming and outgoing quarks, is given by ⁸

⁸The corresponding uncorrelated matrix elements squared for $q\bar{q} \rightarrow t\bar{t}$ are given by $(|\mathcal{A}_{RL}^2| + |\mathcal{A}_{LR}^2|)_{uncorr} = \mathcal{K}_{q\bar{q}}(t \cdot \bar{e})(\bar{t} \cdot \mu)[(p_1 \cdot t)^2 + (p_2 \cdot t)^2 + m_t^2(p_1 \cdot p_2)]$

$$\begin{aligned}
|\mathcal{A}|_{RL}^2 + |\mathcal{A}|_{LR}^2 = & \mathcal{K}_{q\bar{q}} \{ 2(t \cdot \bar{e})(\bar{t} \cdot \mu)[(q \cdot t)^2 + (\bar{q} \cdot t)^2] \\
& - m_t^2[(q \cdot \bar{q})(t \cdot \bar{e})(t \cdot \mu) + (\bar{t} \cdot \bar{e})(\bar{t} \cdot \mu)] \\
& - m_t^2(\bar{e} \cdot \mu) - 2((q \cdot t)(q \cdot \mu)(\bar{q} \cdot \bar{e}) \\
& + (\bar{q} \cdot t)(q \cdot \bar{e})(\bar{q} \cdot \mu) \\
& - (q \cdot t)(\bar{q} \cdot t)(\bar{e} \cdot \mu)) \}. \quad (\text{B1})
\end{aligned}$$

This has the same functional form as the part of Eq. (47) in the second set of curly brackets. The overall factor $\mathcal{K}_{q\bar{q}}$ is

given by

$$\begin{aligned}
\mathcal{K}_{q\bar{q}} = & \frac{2^6 g_s^4}{(q \cdot \bar{q})^2} \frac{g_w^8}{(m_t \Gamma_t)^4} \frac{b \cdot \nu}{(2\bar{e} \cdot \nu - m_w^2)^2 + (m_w \Gamma_w)^2} \\
& \times \frac{\bar{b} \cdot \bar{\nu}}{(2\mu \cdot \bar{\nu} - m_w^2)^2 + (m_w \Gamma_w)^2}. \quad (\text{B2})
\end{aligned}$$

Equations (B1) and (B2) are the Lorentz-invariant equivalents of Eqs. (4) and (5) of Ref. [6].

-
- [1] See talk by Florencia Canelli at Lepton Photon 2009, <http://lp09.desy.de/>.
- [2] G. Mahlon and S.J. Parke, Phys. Rev. D **53**, 4886 (1996).
- [3] T. Stelzer and S. Willenbrock, Phys. Lett. B **374**, 169 (1996).
- [4] A. Brandenburg, Phys. Lett. B **388**, 626 (1996).
- [5] S.J. Parke and Y. Shadmi, Phys. Lett. B **387**, 199 (1996).
- [6] G. Mahlon and S.J. Parke, Phys. Lett. B **411**, 173 (1997).
- [7] W. Bernreuther, A. Brandenburg, and Z.G. Si, Phys. Lett. B **483**, 99 (2000).
- [8] W. Bernreuther, A. Brandenburg, Z.G. Si, and P. Uwer, Phys. Lett. B **509**, 53 (2001).
- [9] W. Bernreuther, A. Brandenburg, Z.G. Si, and P. Uwer, Phys. Rev. Lett. **87**, 242002 (2001).
- [10] W. Bernreuther, A. Brandenburg, Z.G. Si, and P. Uwer, Nucl. Phys. **B690**, 81 (2004).
- [11] M.L. Mangano and S.J. Parke, Phys. Rep. **200**, 301 (1991).
- [12] R. Kleiss and W.J. Stirling, Nucl. Phys. **B262**, 235 (1985).
- [13] M. Hori, Y. Kiyoy, and T. Nasuno, Phys. Rev. D **58**, 014005 (1998).
- [14] P. Uwer, Phys. Lett. B **609**, 271 (2005).
- [15] J. Shelton, Phys. Rev. D **79**, 014032 (2009).
- [16] J. Kodaira, T. Nasuno, and S.J. Parke, Phys. Rev. D **59**, 014023 (1998).
- [17] R.K. Ellis and J.M. Campbell provide us with a special version of MCFM which included all spin correlations for $t\bar{t}$ production at NLO.
- [18] S. Frixione, E. Laenen, P. Motylinski, and B.R. Webber, J. High Energy Phys. 04 (2007) 081; S. Frixione and B.R. Webber, J. High Energy Phys. 06 (2002) 029.
- [19] K. Melnikov and M. Schulze, J. High Energy Phys. 08 (2009) 049.
- [20] M. Jacob and G.C. Wick, Ann. Phys. (N.Y.) **7**, 404 (1959).
- [21] M.E. Rose, *Elementary Theory of Angular Momentum* (John Wiley & Sons, Inc., New York, 1957).
- [22] A.R. Edmonds, *Angular Momentum in Quantum Mechanics* (Princeton University Press, Princeton, 1957), p. 59.
- [23] G. Mahlon and S.J. Parke, Phys. Rev. D **58**, 054015 (1998).
- [24] G. Mahlon and S. Parke, Phys. Rev. D **74**, 073001 (2006).